

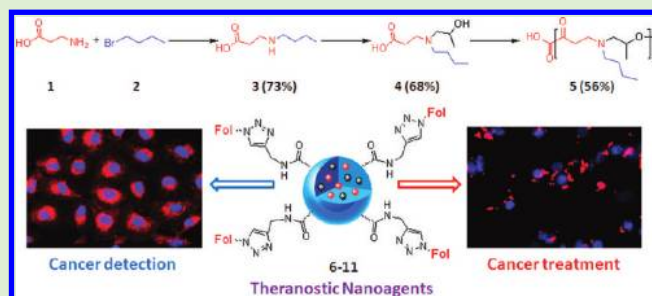
# Selective *N*-Alkylation of $\beta$ -Alanine Facilitates the Synthesis of a Poly(amino acid)-Based Theranostic Nanoagent

Santimukul Santra<sup>\*,†</sup> and J. Manuel Perez<sup>\*,†,‡</sup>

<sup>†</sup>NanoScience Technology Center and <sup>‡</sup>Burnett School of Biomedical Sciences, College of Medicine, Chemistry Department, University of Central Florida, 12424 Research Parkway, Suite 400, Orlando, Florida 32826, United States

**S** Supporting Information

**ABSTRACT:** The development of functional amino acid-based polymeric materials is emerging as a platform to create biodegradable and nontoxic nanomaterials for medical and biotechnology applications. In particular, facile synthetic routes for these polymers and their corresponding polymeric nanomaterials would have a positive impact in the development of novel biomaterials and nanoparticles. However, progress has been hampered by the need to use complex protection–deprotection methods and toxic phase transfer catalysts. In this study, we report a facile, single-step approach for the synthesis of an *N*-alkylated amino acid as an AB-type functional monomer to generate a novel pseudo-poly(amino acid), without using the laborious multistep, protection–deprotection methods. This synthetic strategy is reproducible, easy to scale up, and does not produce toxic byproducts. In addition, the synthesized amino acid-based polymer is different from conventional linear polymers as the butyl pendants enhance its solubility in common organic solvents and facilitate the creation of hydrophobic nanocavities for the effective encapsulation of hydrophobic cargos upon nanoparticle formation. Within the nanoparticles, we have encapsulated a hydrophobic DiI dye and a therapeutic drug, Taxol. In addition, we have conjugated folic acid as a folate receptor-targeting ligand for the targeted delivery of the nanoparticles to cancer cells expressing the folate receptor. Cell cytotoxicity studies confirm the low toxicity of the polymeric nanoparticles, and drug-release experiments with the Taxol-encapsulated nanoparticles only exhibit cytotoxicity upon internalization into cancer cells expressing the folate receptor. Taken together, these results suggested that our synthetic strategy can be useful for the one-step synthesis of amino acid-based small molecules, biopolymers, and theranostic polymeric nanoagents for the targeted detection and treatment of cancer.



## INTRODUCTION

Biodegradable amphiphilic polymers self-assemble into polymeric nanoparticles (PNPs) and polymersomes in aqueous solution and can potentially be used in catalysis, sensing, parenteral drug delivery, and imaging.<sup>1–6</sup> In order to introduce unique properties into these polymeric nanoparticles, a variety of therapeutic cargos have been encapsulated within the polymeric nanocavities.<sup>7–10</sup> Often times, the diversity of the encapsulated cargos is compromised by the nature of the polymeric nanocavities that limits the amount and type of cargo that is encapsulated. Most polymeric matrixes are composed of a hydrophobic core (polymeric backbone) and a large number of polar reactive surface groups.<sup>11–13</sup> The hydrophobic core serves as a reservoir for hydrophobic cargos, whereas the hydrophilic surface can be functionalized for targeting.<sup>14</sup> In particular, aliphatic polymeric nanoparticles have received much attention due to their solubility and biodegradability.<sup>15,16</sup> For example, aliphatic linear polyesters such as poly(L-lactic acid) (PLA), poly(DL-lactic-co-glycolic acid) (PLGA), and poly( $\epsilon$ -caprolactone) (PCL) have been combined with hydrophilic poly(ethylene glycol) (PEG) segments to produce AB-type (A: acidic or electrophilic center; B: basic or nucleophilic center) of

diblock copolymer structures.<sup>17–19</sup> However, the presence of hydrophobic linear pendants in these polymeric structures increases the cavity size of the polymeric core, thereby enhancing the loading of therapeutic cargos. For instance, poly(aspartic acid)–PEG diblock copolymer, an amino acid-based biopolymer, exhibited promising results in encapsulating or chemically conjugating cargos within the polymeric core and has resulted in an effective suppression of tumor growth when injected *in vivo*.<sup>20</sup> This is due to the presence of pendant carboxylated aliphatic chains in the polymer structure, creating large polymeric cavities in the nanostructure for the effective preservation of various cargos. In addition, other amino acid-based biopolymers, such as poly(glutamic acid),<sup>21</sup> poly(aspartic acid),<sup>22</sup> and polyproline dendrimers,<sup>23</sup> are also widely used in biomedical applications due to their enhanced solubility, biocompatibility, and low profile cytotoxicity. Syntheses of such biomacromolecules involve polymerization of an appropriate cyclic monomer<sup>22</sup> or selective  $-\text{NH}_2$  group protection

Received: July 5, 2011

Revised: September 15, 2011

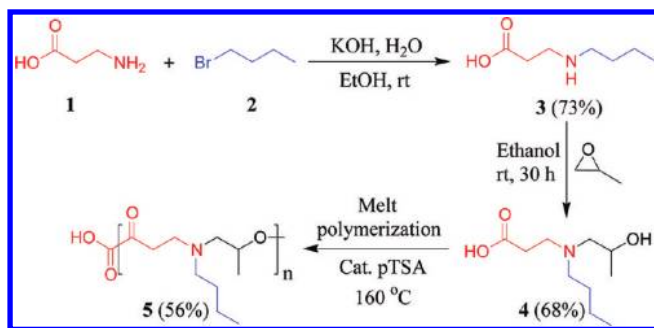
Published: September 30, 2011

and deprotection of the corresponding amino acid. This is due to the fact that direct polymerization of an amino acid often results in the formation of cyclic monomers and cross-linked low molecular weight poly(amino acid)s and oligomers. Furthermore, the interest in developing new protocols for the selective syntheses of mono- and di-*N*-alkylated amino acids and its derivatives is increasing due to their potential applications in creating small molecule-based therapeutic agents and biopolymers.<sup>24,25</sup> Hence, the design and synthesis of functional amino acids for the synthesis of biodegradable branched polymers would provide an ideal platform to develop novel theranostic nanoagents for the effective encapsulation and delivery of therapeutic drugs.

Selective mono- and di-*N*-alkylation of amino acid is an approach that typically is used to functionalize amino acids for further applications. Various methods for the selective *N*-alkylation of amino acids have been reported; however, they often involve multiple reaction steps, resulting in a process that is difficult to scale-up, with low yields and the generation of toxic byproducts that hamper their clinical applications.<sup>26–28</sup> In addition, this process is limited to some amino acids<sup>29</sup> and typically requires the use of time-consuming protection–deprotection protocols<sup>26,30–38</sup> and toxic phase transfer catalysts.<sup>39</sup> On the other hand, *N*-alkylated amino acid facilitates the formation of soluble, high molecular weight polymers upon polymerization, whereas cyclization of the starting monomers, low-molecular weight oligomers, and cross-linked byproducts resulted when a simple amino acid is polymerized. Therefore, there is a great need for a facile, one-step synthetic strategy for the synthesis of selective *N*-alkylated amino acids.

In this paper, we report a facile, one-step strategy for the selective synthesis of mono- and di-*N*-alkylated amino acids, poly(amino acid)s, and Taxol-loaded theranostic polymeric nanoagents for the selective delivery of Taxol for the treatment of cancer. Our strategy is facile, easy to scale-up, and involves no conventional protection–deprotection methods<sup>26,30–38</sup> or phase transfer catalysts.<sup>39</sup> In addition to the one-step selective synthesis of mono-*N*-alkylated amino acids (3, Scheme 1), the

**Scheme 1. Synthesis of Selective Mono- and Di-*N*-alkylated  $\beta$ -Alanine and Its Functional Poly(amino acid)**



present synthetic strategy is also capable of synthesizing novel di-*N*-alkylated functional molecules (4), using a different alkylating agent. Here, we have used this functional molecule (4) as an AB-type linear monomer for the synthesis of a novel pseudo-poly(amino acid) (5).<sup>40,41</sup> Our present study further demonstrates the application of our current strategy by synthesizing novel theranostic nanoagents (6–11) from the resulting polymer and their potential use in the detection and

treatment of cancer. More importantly, the synthesized functional AB monomer is designed in such a way that, when polymerized, the resulting pseudo-poly(amino acid) (5) contains an amphiphilic polyester backbone and hydrophobic butyl pendants in the structure. These aliphatic butyl pendants played an important role in creating hydrophobic nanocavities when solvent diffusion method<sup>14,42</sup> was used to synthesize these polymeric nanoparticles (PNPs). Therefore, the PNP's hydrophobic cavity provides high affinity for the encapsulation of hydrophobic dyes and therapeutic drugs. The nanoparticles' surface carboxylic acid groups can be further functionalize to target and induce delivery of the encapsulated therapeutic agents. Taken together, our one-step green synthetic approach has several advantages: (i) selective mono- and di-*N*-alkylation of amino acids, (ii) synthesis of amino acid-based functional molecules and biodegradable polymers, (iii) easy fabrication of theranostic PNPs in aqueous medium, (iv) "click" chemistry-based surface functionalizations (folate ligand) for cancer targeting, (v) hydrophobic dyes encapsulations for optical detection of cancer, and (vi) therapeutic agent (Taxol)<sup>43–45</sup> encapsulation and delivery for cancer treatment.

## EXPERIMENTAL SECTION

**Materials.** Propylene oxide (PO), butyl bromide (BuBr),  $\beta$ -alanine, potassium hydroxide (KOH), tetrahydrofuran (THF), acetyl chloride, acetonitrile, potassium bromide (KBr), *p*-toluenesulfonic acid (pTSA), *N,N'*-dimethylformamide (DMF), Taxol, 3-(4,5-dimethylthiazol-2-yl)-2,5-diphenyltetrazolium bromide (MTT), *N*-hydroxysuccinimide (NHS), propargylamine, folic acid, porcine liver esterase, ethylenediamine, sodium azide, and other chemicals were purchased from Sigma-Aldrich and used without further purification. Hydrophobic dye (DiI: D282) and 4',6-diamidino-2-phenylindole (DAPI: D1306) were purchased from Invitrogen, whereas the EDC (1-ethyl-3-[3-(dimethylamino)propyl]carbodiimide hydrochloride) was obtained from Pierce Biotechnology. PD-10 columns (Sephadex G-25M) were obtained from GE Healthcare Biosciences. The human lung carcinoma cell line A549 and cardiomyocytes H9c2 were obtained from ATCC. Dialysis cups were obtained from Spectrum Laboratories.

**Synthesis and Characterizations of Mono-*N*-butylated  $\beta$ -Alanine (3-(Butylamino)propionic Acid, 3).**  $\beta$ -Alanine (1, 1.0 g, 11.23 mmol), ethanol (15 mL), and KOH (1.26 g, 22.47 mmol) were taken in a 100 mL round-bottom flask and stirred at room temperature. Water was added to the flask in a dropwise fashion until the reaction mixture became homogeneous. Butyl bromide (2, 1.39 g, 10.11 mmol) was added dropwise to the reaction mixture and stirred at room temperature. The progress of the reaction was monitored by thin layer chromatography (TLC). The reaction mixture was concentrated using a rotary evaporator under reduced pressure. The product was then purified by column chromatography using 12% methanol in chloroform as eluent to get pure colorless viscous liquid. Yield: 1.19 g (73%). <sup>1</sup>H NMR (400 MHz, CDCl<sub>3</sub>,  $\delta$  ppm, *J* Hz): 0.94 (t, 3H, *J* = 7.3), 1.42 (m, 2H), 1.73 (m, 2H), 2.53 (t, 2H, *J* = 6.1), 2.92 (t, 2H, *J* = 7.6), 3.09 (t, 2H, *J* = 5.8), 8.85 (bs, 1H). <sup>13</sup>C NMR (100.56 MHz, CDCl<sub>3</sub>,  $\delta$  ppm): 13.49, 19.82, 28.04, 31.84, 44.46, 46.57, 176.74. IR (CHCl<sub>3</sub>): 3414, 2961, 2870, 2448, 1711, 1578, 1464, 1394, 1304, 1198, 1137, 1037, 932, 847, 692, 597 cm<sup>-1</sup>. Q-tof high-resolution mass spectrometry (HRMS): Calculated mass for C<sub>7</sub>H<sub>16</sub>NO<sub>2</sub> is 146.1181. Found: 146.1184.

**Synthesis and Characterizations of di-*N*-butylated  $\beta$ -Alanine (3-(Dibutylamino)propionic Acid, 3A).**  $\beta$ -Alanine (1, 1.0 g, 11.23 mmol), ethanol (15 mL), and KOH (1.89 g, 33.71 mmol) were taken in a 100 mL round-bottom flask and stirred at room temperature. Water was added to the flask in a dropwise fashion until the reaction mixture became homogeneous. Butyl bromide (2, 3.54 g, 25.84 mmol) was added dropwise to the reaction mixture and stirred at room temperature. The progress of the reaction was monitored by TLC. The reaction mixture was concentrated using rotary evaporator under

reduced pressure. The product was then purified by column chromatography using 10% methanol in chloroform as eluent to get pure colorless viscous liquid. Yield: 1.46 g (65%).  $^1\text{H NMR}$  (400 MHz,  $\text{CDCl}_3$ ,  $\delta$  ppm, J Hz): 0.95 (t, 6H,  $J = 7.4$ ), 1.37 (m, 4H), 1.60 (m, 4H), 2.50 (t, 2H,  $J = 6.4$ ), 2.78 (t, 4H,  $J = 8.2$ ), 2.98 (t, 2H,  $J = 6.4$ ), 10.14 (bs, 1H).  $^{13}\text{C NMR}$  (100.56 MHz,  $\text{CDCl}_3$ ,  $\delta$  ppm): 13.55, 20.07, 25.79, 30.42, 49.70, 51.56, 174.78. IR ( $\text{CHCl}_3$ ): 3399, 2944, 2831, 2516, 2226, 2044, 1708, 1606, 1450, 1202, 1119, 1027, 714  $\text{cm}^{-1}$ . Q-tof high-resolution mass spectrometry (HRMS): Calculated mass for  $\text{C}_{11}\text{H}_{24}\text{NO}_2$  is 202.1807. Found: 202.1814.

**Synthesis and Characterizations of 3-[Butyl-(2-hydroxypropyl)amino]propionic Acid (4).** 3-(Butylamino)propionic acid (3, 2.0 g, 13.79 mmol) and commercial ethanol (20 mL) were taken in a round-bottom flask and stirred at room temperature. Propylene oxide (1.6 g, 27.58 mmol) was added dropwise to the reaction mixture and stirred at room temperature. The progress of the reaction was monitored by TLC. The reaction mixture was evaporated using rotary evaporator under reduced pressure to get the pure compound as a viscous liquid. Yield: 1.90 g (68%).  $^1\text{H NMR}$  (400 MHz,  $\text{CDCl}_3$ ,  $\delta$  ppm, J Hz): 0.95 (t, 3H,  $J = 7.4$ ), 1.21 (d, 3H,  $J = 6.4$ ), 1.37 (m, 2H), 1.67 (m, 2H), 2.00 (s, 1H), 2.59 (m, 2H), 2.95 (m, 2H), 3.07 (m, 2H), 3.26 (m, 2H), 4.18 (m, 1H), 9.19 (bs, 1H).  $^{13}\text{C NMR}$  (100.56 MHz,  $\text{CDCl}_3$ ,  $\delta$  ppm): 13.64, 19.99, 21.10, 25.41, 30.83, 51.16, 53.22, 60.63, 61.65, 175.58. IR ( $\text{CHCl}_3$ ): 3414, 2965, 2935, 2876, 2571, 2239, 1715, 1593, 1459, 1382, 1196, 1141, 1088, 1009, 912, 845, 732, 644, 600  $\text{cm}^{-1}$ . Q-tof high-resolution mass spectrometry (HRMS): Calculated mass for  $\text{C}_{10}\text{H}_{22}\text{NO}_3$  is 204.1600. Found: 204.1601.

**Synthesis and Characterizations of the Polymer 5.** 3-[Butyl-(2-hydroxypropyl)amino]propionic acid (4) and the catalyst *p*-toluenesulfonic acid (100:1 molar ratio) were taken in a polymerization vessel, and the polymerization reaction was carried out under dry argon gas atmosphere. Then the reaction vessel was slowly heated to 160 °C using an oil bath and kept at this temperature for 4 h. The evolution of the byproduct, water vapor, was clearly visible from the reaction vessel, confirming the progression of the polymerization reaction. The reaction mixture was then evacuated by applying vacuum at 0.2 mm/Hg for 2 h while maintaining the same polymerization temperature. The resulting polymer was found to be soluble in DMF, DMSO, chloroform, and insoluble in water and acetone. The polymer was purified by precipitating into acetone from its chloroform solution. This was then centrifuged, washed with solvent, and dried in a vacuum oven to get pure polymer. Yield: 56%.  $^1\text{H NMR}$  (400 MHz,  $\text{CDCl}_3$ ,  $\delta$  ppm): 0.90 (m, 3H), 1.28 (m, 5H), 1.46 (m, 2H), 2.07 (s, 1H), 2.52 (m, 2H), 2.82 (m, 2H), 3.52 (m, 2H), 4.72 (m, 1H).  $^{13}\text{C NMR}$  (100.56 MHz,  $\text{CDCl}_3$ ,  $\delta$  ppm): 13.66, 19.82, 20.59, 21.79, 25.82, 29.24, 30.82, 31.58, 49.06, 50.69, 52.65, 54.77, 61.61, 67.78, 170.88. IR ( $\text{CHCl}_3$ ): 3300, 2960, 2933, 2873, 1731, 1638, 1563, 1457, 1379, 1239, 1187, 1122, 1034, 919, 817, 682, 644, 568  $\text{cm}^{-1}$ . SEC ( $\text{CHCl}_3$ ):  $M_w = 58\,700$ , PDI = 1.6.

#### Characterization of Synthesized Monomers and Polymer.

Infrared spectra were recorded on a PerkinElmer Spectrum 100 FT-IR spectrometer in chloroform. UV/vis spectra were recorded using CARY 300 Bio UV/vis spectrophotometer. Fluorescence spectra were recorded on a NanoLog Horiba jobin Yvon fluorescence spectrophotometer. NMR spectra were recorded on a Varian 400 MHz spectrometer using the TMS/solvent signal as an internal reference. Q-tof Micro mass experiments (HRMS) were carried out using Waters Q-Tofmicro-YA-105.

**Size Exclusion Chromatography (SEC).** The molecular weight of the resulting polymer (5) was determined using size exclusion chromatography (SEC), using a JASCO MD 2010 Plus instrument with a PD 2020 light scattering precision detector. The average molecular weight was calculated against a polystyrene standard, using HPLC-grade chloroform as the mobile phase. The average molecular weight of the polymer 5 was  $M_w = 58\,700$ , PDI = 1.6. Degradation experiment of this polymer was performed using porcine liver esterase in solution. After 24 h of incubation at 37 °C, the average molecular weight of the resulting low molecular weight polymers and oligomers were found to be  $M_w = 21\,300$ , PDI = 2.3.

**Thermogravimetric Analysis (TGA).** The thermal stability of the synthesized pseudo-poly(amino acid) (5) was measured using thermogravimetric analysis. This experiment was performed on a SETARAM, Mettler TC11 instrument with sample sizes of 10–20 mg. All experiments were done using a heating rate of 10 °C/min in air.

**Synthesis and Characterizations of DiI Dye-Encapsulating Polymeric Nanoparticles (6).** *Water-Based Solvent Diffusion Method.* 1.2 mg of DiI dye in 250  $\mu\text{L}$  of DMF was mixed in 250  $\mu\text{L}$  of DMF solution containing polymer 5 (25 mg) and vortexed. The resulting polymer–DiI mixture in DMF was added dropwise to deionized water (5 mL) with continuous stirring at room temperature forming DiI-encapsulating PNPs (6). The synthesized PNPs (6) were purified using a PD-10 column and finally dialyzed (MWCO 6K–8K) against PBS (pH = 7.4).

#### Synthesis of Taxol and DiI Coencapsulating PNPs (7).

Similarly, 1.5 mg of Taxol and 0.25 mg of DiI dye in 250  $\mu\text{L}$  of DMF were mixed with carboxylated polymer 5 (25 mg) in 250  $\mu\text{L}$  of DMF and followed the solvent diffusion method as described above.

#### Synthesis of Propargylated Polymeric Nanoparticles (8, 9).

Carbodiimide chemistry was used following the previously reported method.<sup>14,46,47</sup> Briefly, to a solution of carboxylated PNPs (6 or 7, 1.0 mmol) in PBS (pH = 7.4), a solution of EDC (10 mmol) and NHS (10 mmol) in MES buffer (pH = 6.0) was added followed by 3 min incubation at room temperature. Propargylamine (10 mmol) in DMF was then added dropwise and continued for 3 h to obtain 8 or 9, respectively. The synthesized functional PNPs were purified using a PD-10 column and finally dialyzed (MWCO 6K–8K) against PBS buffer (pH = 7.4). They were stored in refrigerator for further characterization.

**Synthesis of Folate-Conjugated Polymeric Nanoparticles (10, 11).** “Click” chemistry was used following previously reported methods.<sup>14,46,47</sup> Briefly, the alkynated PNPs 8 or 9 ( $6 \times 10^{-3}$  mmol) in bicarbonate buffer (pH = 8.5) were taken to an Eppendorf containing catalytic amount of CuI ( $6 \times 10^{-10}$  mmol) in 250  $\mu\text{L}$  of bicarbonate buffer (pH = 8.5) and vortexed. To the resulting solution, azide-functionalized folic acid<sup>14,46,47</sup> ( $6 \times 10^{-2}$  mmol) in DMSO was added, and the reaction was incubated at room temperature for 12 h. The synthesized PNPs (10, 11) were purified using a PD-10 column and finally dialyzed (MWCO 6K–8K) against PBS solution (pH = 7.4). The number of folate molecules per nanoparticle was found to be  $23 \pm 4$ , following a protocol described before.<sup>14</sup> They were stored in refrigerator for further characterization.

**Drug and Dye Encapsulation Efficiency.** The nanoparticles were digested in a slightly acidic DI water (pH = 6.0–6.5) to release encapsulated cargos. The presence of a trace amount of diluted HCl was removed by applying nitrogen flow overnight. The analysis on the assays of Taxol and DiI dye were determined by high-performance liquid chromatography (HPLC, PerkinElmer 200 series) at the detection wavelength of 227 nm and by standard UV/vis spectroscopic method at the detection wavelength of 553 nm, respectively. Standard calibration curves for free Taxol and DiI dye were plotted by performing HPLC and UV/vis experiments with different concentrations of Taxol and DiI dye, respectively. HPLC chromatograms of free Taxol and Taxol-encapsulating nanoparticles presented in the Supporting Information (Figure S8) showed the successful encapsulation of the drug. The Taxol and DiI dye encapsulation efficiencies (EE%) in polymeric nanoparticle (11) were found to be  $68.5 \pm 3.2\%$  and  $21.2 \pm 1.3\%$ , respectively.

**Size and Zeta Potential of PNPs.** The size and dispersity of the synthesized functional PNPs was measured using dynamic light scattering (DLS) using PDDLS/CoolBatch 40T instrument with Precision Deconvolve 32 software. The overall surface charge (zeta potential) of functional PNPs was measured using a Zetasizer Nano ZS from Malvern Instruments.

**Cell Cultures.** The human lung carcinoma (A549) and cardiomyocyte (H9c2) cells were obtained from ATCC and maintained in accordance to the supplier's protocols. Briefly, the lung carcinoma cells were grown in a 5% FBS-containing DMEM medium supplemented with L-glutamine, streptomycin, amphotericin B, and sodium bicarbonate. The H9c2 cells were propagated in a 10%

FBS-containing MEM medium containing penicillin, streptomycin, and bovine insulin (0.01 mg/mL). Cells were grown in a humidified incubator at 37 °C under 5% CO<sub>2</sub> atmosphere.

**Cytotoxicity Assay.** H9c2 and A549 cells (2500 cells/well) were seeded in 96-well plates, incubated with the corresponding PNPs (35 μL, 5.8 nM, in PBS pH = 7.4) at 37 °C. After 24 h of incubation, each well was washed three times with 1X PBS and treated with 30 μL MTT (2 μg/μL) for 2 h. The resulting formazan crystals were dissolved in acidic isopropanol (0.1 N HCl), and the absorbance was recorded at 570 and 750 nm (background), using a Synergy μQuant microtiter plate reader (Biotek). These experiments were performed in triplicates.

**Fluorimetric Assessment of *in Vitro* Cellular Internalization and Apoptosis.** Folate-receptor positive cells (A549) and negative cells (H9c2) were seeded to reach confluency in a Costar's black polystyrene 96-well plate. The cells were treated with functional PNPs (35 μL, 5.8 nM) in PBS (pH = 7.4), and after 24 h of incubation, the cells were washed three times with 1X PBS. Subsequently, 1 mL of 1X PBS was added to each well and fluorescence emission acquisition using the TECAN's infinite M200 PRO fluorescence plate reader.

**Confocal Laser-Scanning Microscopy.** H9c2 and A549 cells were grown overnight on culture dishes, before treatment. Cells (10 000 cells/well) were incubated with the corresponding functional PNPs (100 μL, 5.8 nM, in PBS pH = 7.4) in a humidified incubator (37 °C, 5% CO<sub>2</sub>). After 24 h of incubation, the cells were thoroughly washed three times with 1X PBS and fixed with 10% formalin solution, followed by nuclear staining with DAPI, which was performed as recommended by the supplier. Then, multiple confocal images were obtained using a Zeiss LSM 510 confocal microscope equipped with a 40× objective.

***In Vitro* Drug Release from Polymeric Nanoparticles.** The *in vitro* drug release studies were carried out using a dynamic dialysis technique at 37 °C. Briefly, 100 μL of Taxol-encapsulating PNPs (11, 5.8 nM) were incubated with porcine liver esterase (20 μL) inside a small dialysis cup (MWCO 6000–8000), which was then placed in a PBS solution (pH 7.4). The amount of Taxol molecules released from the nanoparticles into the PBS solution was determined at regular time intervals by taking 1 mL aliquots from the PBS solution and measuring the fluorescence intensity at 378 nm for Taxol. The cumulative fraction of release versus time was calculated using the following equation:

$$\text{cumulative release (\%)} = [\text{Taxol}]_t / [\text{Taxol}]_{\text{total}} \times 100$$

where  $[\text{Taxol}]_t$  is the amount of Taxol released at time  $t$  and  $[\text{Taxol}]_{\text{total}}$  is the total Taxol present in the Taxol-encapsulating PNPs.

**Flow Cytometry.** Flow cytometry was done to assess the fluorescence enhancement of our PNPs when folate-receptor-expressing A549 cells were incubated with the functional PNPs in a humidified incubator at 37 °C under 5% CO<sub>2</sub> atmosphere. Cells were seeded to reach confluency in Petri dishes and treated with functional PNPs (100 μL, 5.8 nM), and after 24 h of incubation the cells were harvested after trypsinization and centrifugation at 1000 rpm for 8 min. Subsequently, the cell pellets were resuspended in 1 mL of 1X PBS, and flow cytometry was done using a BD FACSCalibur flow cytometer from BD Biosciences.

## RESULTS AND DISCUSSION

**Syntheses of Selective Mono- and Di-*N*-alkylated Amino Acids and Functional Poly(amino acid).** In our novel one-step method, we used two different miscible solvents, water and ethanol, to facilitate the formation of a homogeneous reaction mixture containing the starting materials (mixed-solvent approach).<sup>48</sup> This eliminates the use of a toxic phase transfer catalyst (PTC) required to bring the starting materials to one phase for the reaction to take place. We selected a water-soluble amino acid, β-alanine (1), and a water-insoluble alkylating agent, butyl bromide (2), as starting materials for the selective *N*-alkylation of β-alanine (Scheme

1). In a typical reaction, β-alanine (1) and KOH were taken in ethanol at room temperature, and a minimum amount of water was added in a dropwise fashion with continuous stirring until all reactants got solubilized in the reaction medium. Afterward, butyl bromide (2) was added slowly to the resulting homogeneous reaction mixture and the stirring continued until the desired reaction time at room temperature. By systematically changing the reaction time and equivalent ratios of the starting materials, we obtained mono- and disubstituted products in different ratios. Therefore, to optimize this facile and one-step synthetic strategy, reactions were carried out under various reaction conditions (Scheme 2). We noticed that

**Scheme 2. Selective Mono- and Di-*N*-alkylation of β-Alanine with Butyl Bromide under Various Conditions**

Entry	Time (h)	Equivalent ratio			% of yield		
		β-Alanine	C <sub>4</sub> H <sub>9</sub> Br	KOH	3	3A	3B
I	16	1	0.9	2	73	~1	-
II	24	1	0.9	2	62	8	-
III	24	1	2.3	2	49	20	-
IV	24	1	2.3	3	11	58	~1
V	36	1	2.3	3	~1	65	~2
VI	24	1	5	6	~1	16	75

when 2 equiv of KOH and 0.9 equiv of 2 reacted with 1 equiv of 1, monosubstituted product 3 resulted as a major product (73%), after 16 h of incubation and performing flash column chromatography using 10% methanol in chloroform as eluent (entry I). This is an optimized reaction condition for the synthesis of mono-*N*-butylated β-alanine (3), minimizing the production of di-*N*-butylated β-alanine (3A) as a side product. Similarly, when the equivalent ratio of 2 and KOH increased to 2.3 and 3.0, respectively, disubstituted product 3A was obtained as a major yield (65%), after 36 h of incubation (entry V) and purifications. The formation of either mono- or di-*N*-substituted β-alanine as a side product was observed and easily purified using flash column chromatography. The synthesis of pure mono- and di-*N*-butylated β-alanine was confirmed by FT-IR, NMR, and mass spectroscopic methods (Figure 1 and Figures S1–S3). In addition, when excess of starting materials were used, the tri-*N*-substituted β-alanine salt (3B) yielded as a major product (entry VI). These results further indicated that the product's selectivity depends on the equivalent ratios of the starting materials and reaction time. Taken together, our one-step method is facile, easy to scale-up, reproducible, and uses a simple mixed-solvent approach to eliminate the use of toxic phase transfer catalysts (PTC). In addition, this strategy does not use any conventional protection–deprotection method, as the selectivity of the *N*-substitution reaction (mono- or di-) was monitored with the equivalent ratios of the starting materials. This synthetic strategy was used for the synthesis of functional di-*N*-alkylated β-alanine (4), capable of producing a pseudo-poly(amino acid) polymer (5, Scheme 1).

Acknowledging the benefit of our one-step method, we designed a synthetic strategy to prepare novel di-*N*-alkylated β-alanine using two different types of alkylating agents, without using any protection–deprotection steps. We hypothesized that

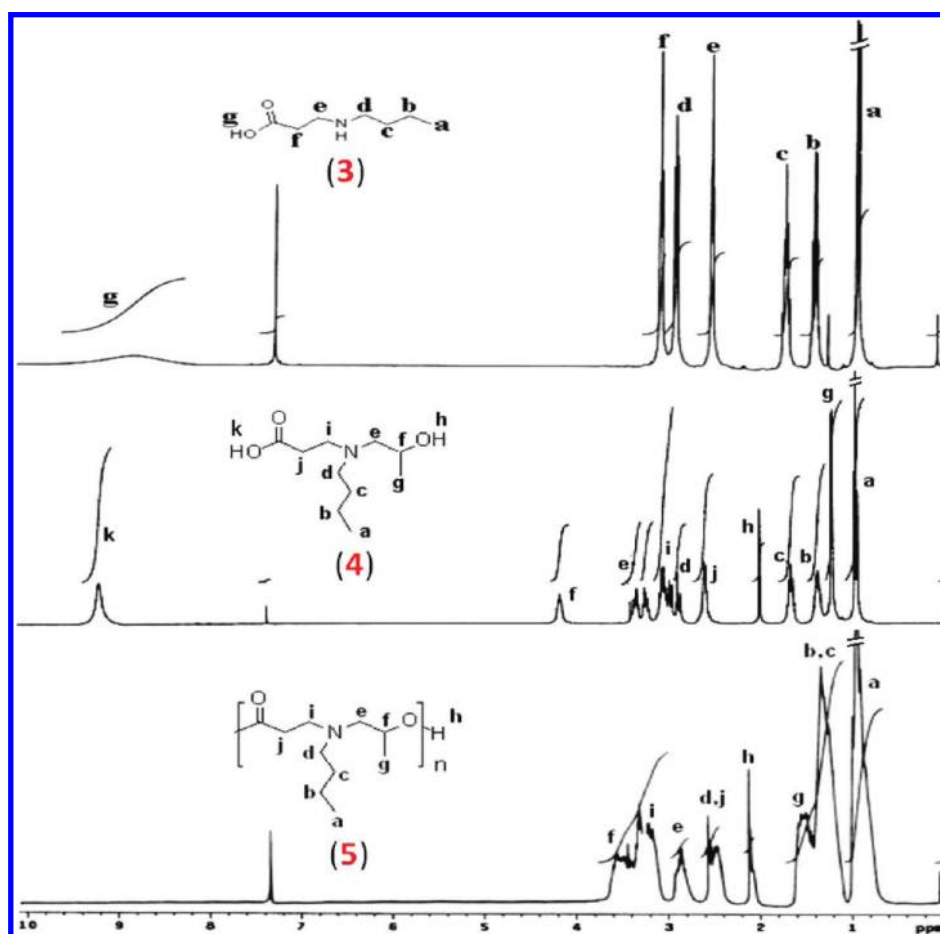


Figure 1. <sup>1</sup>H NMR spectra of the monomers (3 and 4) and the pseudo-poly(amino acid) (5).

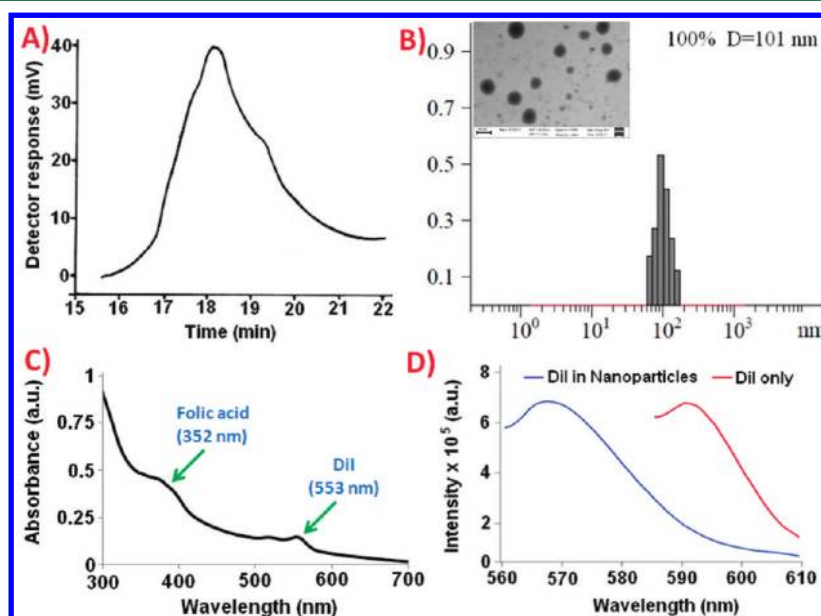
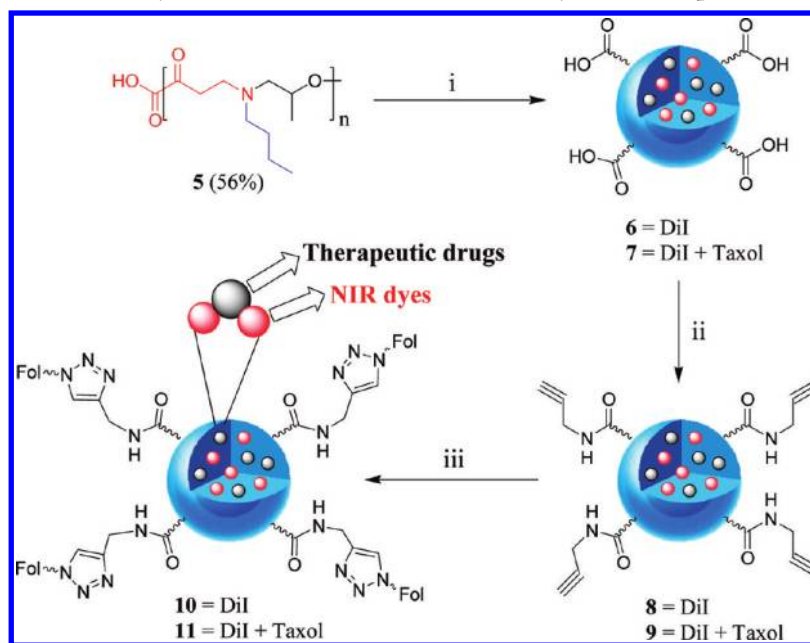


Figure 2. Characterizations of polymer 5 and polymeric nanoparticles. (A) SEC trace of polymer 5 in chloroform, showing formation of high molecular weight polymer. (B) DLS measurement determines the average hydrodynamic diameter ( $101 \pm 2$  nm) of PNPs 10. Inset: scanning transmission electron microscopy (STEM) image of PNPs 10. Scale bar 100 nm. (C) UV/vis spectrum indicating the presence of DiI and folic acid and (D) comparing fluorescence emission spectra of DiI in PNPs 10 with that of free DiI dye in PBS (pH = 7.4).

the design and synthesis of functional di-*N*-alkylated  $\beta$ -alanine monomer would be a versatile precursor for the synthesis of novel biopolymers. In addition, the presence of a butyl

pendant will enhance the solubility of the resulting polymer in common organic solvents. Furthermore, the butyl pendant will create a pseudo-branched structure upon

Scheme 3. Synthesis of Functional Poly(amino acid)-Based Theranostic Polymeric Nanoparticles<sup>a</sup>

<sup>a</sup>i. Solvent diffusion method, DMF, H<sub>2</sub>O, DiI, Paclitaxel. ii. Carbodiimide chemistry, propargylamine, EDC, NHS. iii. Click chemistry, Folate~N<sub>3</sub>, CuI.

polymerization due to the hydrophobic–hydrophobic interactions, hinting the formation of hydrophobic nanocavities in the polymeric nanostructure. As hypothesized, we started with monobutylated β-alanine (**3**) as an important ethanol soluble precursor and a typical nucleophilic substitution reaction was performed with the addition of a different alkylating agent, propylene oxide, in ethanol. The reaction was continued for 30 h at room temperature to obtain the pure di-*N*-alkylated β-alanine (**4**, Scheme 1), the AB-type of butyl-functional monomer in high yield (68%). Importantly, this reaction did not require any work-up step or column purification due to the evaporation of low-boiling (34 °C) propylene oxide from the reaction mixture, while concentrating the reaction mixture. In addition, this step neither uses water as a cosolvent since the reactants were soluble in ethanol nor uses any bases for the reaction to proceed, as the starting material (**3**) contains a highly nucleophilic secondary amine group. The resulting bifunctional derivative (**4**) was polymerized using the melt-polymerization technique<sup>14,42</sup> in the presence of *p*-toluenesulfonic acid (pTSA) as a catalyst at 160 °C. Importantly, the melt-polymerization technique does not require any surfactants, used for microemulsion polymerization,<sup>49</sup> indicating the formation of pure polymer. As hypothesized, the resulting amino acid-based biodegradable<sup>13,15</sup> polymer (**5**) was found to be soluble in chloroform, DMF, and DMSO and insoluble in water and acetone. The polymer was purified by precipitating in acetone from a chloroform solution and isolated as pure polymer with high yield (56%). The synthesized amino acid derivatives and polymer were characterized using spectroscopic methods (Figure 1 and Figures S1–S4), and the formation of polymer was further confirmed by size exclusion chromatography (SEC:  $M_w = 58\,700$ , PDI = 1.6; Figure 2A). Thermal gravimetric analysis (TGA) showed the moderate thermal stability of the synthesized polymer (10% weight loss at 253 °C in air), indicating the formation of a potentially degradable polymer<sup>16</sup> (Figure S5). In addition, the degradability of our

polymer was further confirmed by SEC experiment after incubation with porcine liver esterase that resulted in the formation of low molecular weight polymers and oligomers (Figure S6). In addition, compared to the conventional linear polymers, our pseudo-poly(amino acid) is amorphous, soluble, biocompatible, containing numerous functional groups, and possessing the ability to form hydrophobic cavities important for effective encapsulation of therapeutic agents, indicated its versatility in targeted drug delivery. Therefore, the synthesized pseudo-poly(amino acid) (**5**) was used to create a series of functional PNPs (**6–11**) containing various cargos and functional groups.

**Syntheses and Characterizations of Cargos-Encapsulating Functional PNPs.** For the synthesis of our cargo-encapsulating PNPs, we used a surfactant-free, water-based solvent diffusion method<sup>14,42</sup> (Scheme 3). In this method, we coencapsulated a hydrophobic fluorescent dye (DiI, 0.25 mg) and a therapeutic drug (Taxol, 1.5 mg) during the formation of PNPs, in one pot. Briefly, the polymer (**5**, 25 mg) and cargos were dissolved in DMF and added dropwise to the stirring DI water (5 mL), driving both the self-assembly of hydrophobic butyl pendants and encapsulation process in one-pot, creating cargo-encapsulating PNPs (**6**, **7**). In this process, the polymer **5** self-assembles to form nanoparticles, bringing the hydrophobic butyl pendants together to minimize the contact with water, while exposing the polar carboxylic acid groups toward the aqueous media for further functionalizations. Next, the resulting carboxylated PNPs (**6**, **7**; Scheme 3) were functionalized to yield propargylated nanoparticles (**8**, **9**) using water-soluble carbodiimide chemistry.<sup>46</sup> Then, highly selective “click” chemistry<sup>50–54</sup> was used to generate folate-functionalized multimodal PNPs (**10**, **11**), using azide-derivatized folic acid.<sup>46</sup> These PNPs (**6–11**) were purified using PD-10 column followed by dialysis (MWCO 6K–8K) against PBS buffer (pH = 7.4). Nanoparticles were found to be highly stable in aqueous buffer solution (pH = 7.4), without significant precipitation or

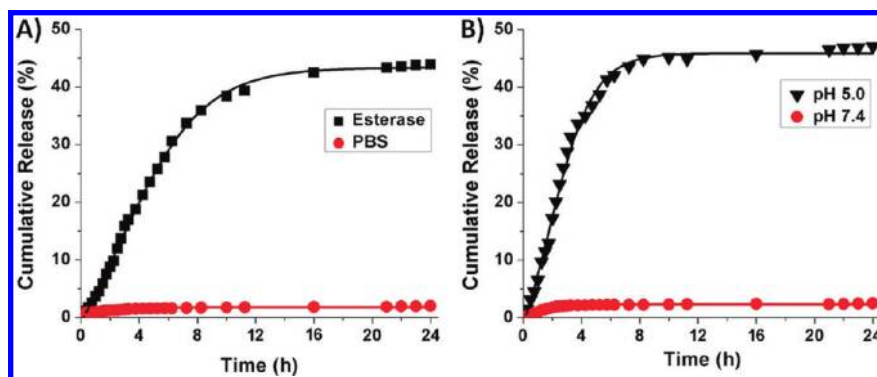


**Figure 3.** Drug release profiles of folate-conjugated Taxol-encapsulating PNPs (**11**, 100  $\mu$ L, 5.8 nM) at 37  $^{\circ}$ C. Release of Taxol were observed in the presence of an esterase enzyme (A,  $\blacksquare$ ) and in PBS at pH 5.0 (B,  $\blacktriangledown$ ), whereas the encapsulating drug was found to be stable in PBS at pH 7.4 (A and B,  $\bullet$ ).

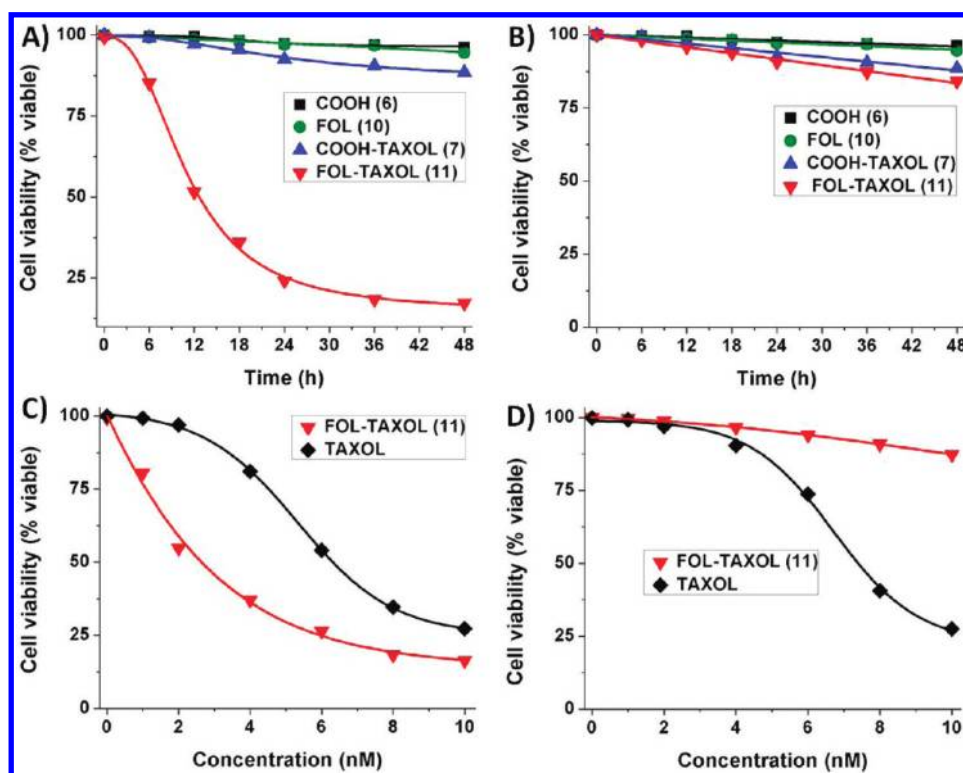


**Figure 4.** Determination of cytotoxicity of functional PNPs (35  $\mu$ L, 5.8 nM in PBS, pH = 7.4): (A, B) Time-dependent and (C, D) dose-dependent viabilities of A549 cells (A, C) and H9c2 cells (B, D) treated with the functional PNPs. Carboxylated (**6**,  $\blacksquare$ ), Taxol-encapsulating carboxylated (**7**,  $\blacktriangle$ ), and folate-conjugated (**10**,  $\bullet$ ) nanoparticles showed biocompatibility with nominal toxicity in both the cell lines. The Taxol-encapsulating folate-conjugated PNPs (**11**,  $\blacktriangledown$ ) showed more than 90% reduction in cell viability when treated with A549 cells (A) and not with H9c2 cells (B), confirming folate-receptor mediated internalizations. Cells were incubated with PNPs **11** and Taxol (1:1 equiv of Taxol concentrations) for 24 h (C, D), and average values of four measurements are depicted  $\pm$  standard errors.

reduction in the fluorescence emission when concentrated (Table S1).

Dynamic light scattering (DLS) experiments confirmed the formation of stable and monodispersed PNPs (**10** in PBS, pH = 7.4) with an average diameter ( $D$ ) of  $101 \pm 2$  nm (Figure 2B). The presence of an absorption maximum at 553 nm in the UV/vis spectrum (Figure 2C) and a corresponding fluorescence emission peak at 568 nm (Figure 2D) confirmed the effective encapsulation of DiI dye ( $EE = 59.2 \pm 5.8\%$ ) in the PNPs **10**. Encapsulation of this cargo inside the PNP's cavity was further confirmed by observing a blue shift<sup>14,55,56</sup> of 22 nm (Figure 2D) after encapsulating DiI dye as compared to the free dye (590 nm) in PBS (pH = 7.4). Surface functionalization was

confirmed by measuring the overall surface charge ( $\zeta$ -potential, Figure S7) and by UV/vis spectroscopy showing an absorption maximum at 352 nm (Figure 2C) for the conjugated folic acid. The presence of encapsulated Taxol ( $EE = 68.5 \pm 3.2\%$ ), DiI dye ( $EE = 21.2 \pm 1.3\%$ ),<sup>17,57–63</sup> and surface-clicked folic acid ( $23 \pm 4$ /PNP) in the PNPs **11** was further confirmed by HPLC (Figure S8) and spectroscopic techniques (Figure S9).

**In Vitro Release of Taxol from Nanoparticles.** To investigate the potential therapeutic applications of our functional PNPs, which rely on their biodegradability, the rate of release of the encapsulated drug (Taxol) from the polymeric nanocavities was studied. To evaluate the PNPs' (**11**, 100  $\mu$ L, 5.8 nM) drug release profile, we performed enzymatic

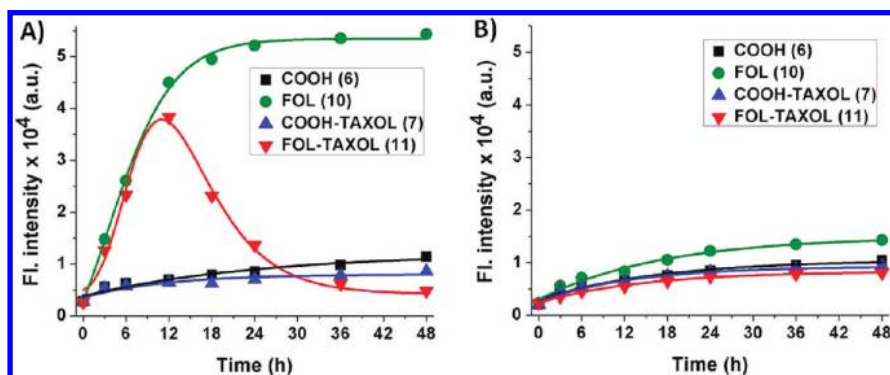


**Figure 5.** Time-dependent intracellular differential fluorescence emissions from A549 cells (A) and H9c2 cells (B) treated with novel functional PNPs ( $35 \mu\text{L}$ ,  $5.8 \text{ nM}$  in PBS,  $\text{pH} = 7.4$ ).

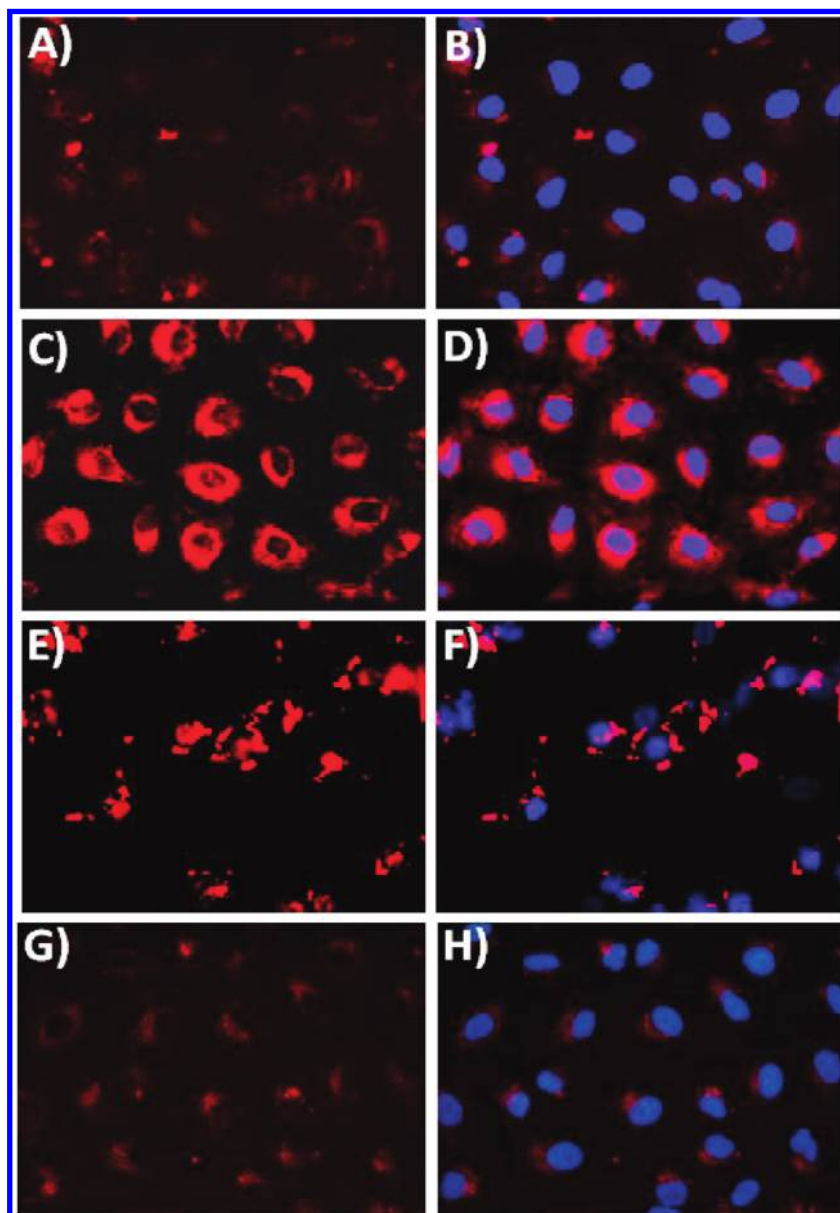


**Figure 6.** *In vitro* assessment of amino acid-based functional PNP's ( $100 \mu\text{L}$ ,  $5.8 \text{ nM}$ , in PBS  $\text{pH} = 7.4$ ,  $24 \text{ h}$ ) cellular uptake via confocal microscopy using A549 cells ( $10\,000$  cells/well). (A, B) Very nominal internalization was observed for carboxylated PNPs (6). (C, D) Enhanced internalization was indicated for folate-conjugated PNPs (10). (E, F) Induced cell death was observed when treated with Taxol-encapsulating PNPs (11). (G, H) No significant internalization was observed when A549 cells were preincubated with excess of free folic acid, before incubation with folate-conjugated PNPs 10. Nucleus stained with DAPI (blue).

(esterase from porcine liver) and low-pH (pH = 5.0) degradation experiments using a dynamic dialysis technique<sup>14,46,47</sup> at 37 °C. Results indicated that Taxol was released faster in the case of low-pH release method (▼, Figure 3B), when compared to the enzymatic release (■, Figure 3A). These differential release profiles may be attributed to the faster rate of hydrolysis (degradation) of the ester linkages present in the polymeric backbone of the polymer 5 at low pH.<sup>64</sup> As nominal drug release was observed at physiological pH 7.4 (●), we deduced that our functional PNPs should be stable under these physiological conditions (Table S1), whereas they are readily biodegraded upon enzymatic and intracellular environmental triggers, such as localization in acidified lysosomal compartments. Taken together, these results confirm the efficient drug release capability of our theranostic PNPs, rendering targeted PNPs' useful for potential *in vivo* applications.

**In Vitro Cytotoxicity of Cargo-Encapsulating Functional PNPs.** After evaluating the rate of release of the encapsulating drug from the polymeric nanocavities, we examined the *in vitro* cytotoxicity of the functional PNPs (35 μL, 5.8 nM in PBS, pH = 7.4) using MTT assay. In this experiment, we used lung carcinoma cells (A549, 2500 cells/well) expressing folate receptor (FR +)<sup>14,65–67</sup> to compare the cytotoxicities of our functional PNPs. Results confirmed that a time-dependent decrease in the number of viable A549 cells, when incubated with folate-decorated Taxol-encapsulating PNPs (11, ▼, Figure 4A). Within 48 h of incubation, the folate-decorated Taxol-encapsulating PNPs 11 (▼) showed more than 90% reduction in cell viability whereas, PNPs 6 (■), 7 (▲), and 10 (●) exhibited nominal cytotoxicities. In contrast, when incubated with cardiomyocytes (H9c2 cells, 2500 cells/well), which do not overexpress folate receptor (FR –),<sup>68</sup> no significant cell death was observed with all the functional PNPs including folate-conjugated Taxol-encapsulating PNPs 11 (▼, Figure 4B). These results demonstrate the biocompatibility, folate-receptor-mediated internalization and the potential application of our theranostic nanoagents for the targeted treatment of folate receptor-expressing tumors. In another set of experiments, dose-dependent cell viability experiments confirmed the higher cytotoxicity of our folate-decorated Taxol-encapsulating PNPs 11 (▼, IC<sub>50</sub> = 2.1 nM) when compared with the similar concentrations of free Taxol (◆, IC<sub>50</sub> = 5.2 nM) in A549 cells (Figure 4C). This is due to the higher rate of folate receptor-mediated internalization of our folate-decorated Taxol-encapsulating PNPs 11, when compared to the nonspecific internalization of free Taxol. On the other hand, the folate-decorated Taxol-encapsulating PNPs 11 (▼) showed very nominal dose-dependent cytotoxicity in H9c2 cells, as these cells lack folate receptor (Figure 4D). In contrast, Taxol exhibits nonselective cytotoxicity (◆, IC<sub>50</sub> = 6.9 nM, Figure 4D), irrespective of the presence of folate receptor for cellular internalization. Overall, these findings support the principle that folate-decorated Taxol-encapsulating PNPs 11 (▼) can target and deliver chemotherapeutic agents to folate receptor-expressing carcinomas, while visualizing the drug's homing.

**Intracellular Fluorescence Emissions and Selective Cytotoxicity.** To further demonstrate the targeted internalization of our theranostic PNPs and its internalization causing cell death, A549 (FR +) and H9c2 (FR –) cells (2500 cells/well) were treated with functional PNPs (35 μL, 5.8 nM in PBS, pH = 7.4). The resulting differential fluorescence

emissions were measured at different time points using a fluorescence microtiter plate reader. Results showed faster internalizations and enhanced fluorescence emissions from A549 cells incubated with folate-conjugated PNPs 10 (●, Figure 5A), reaching a maximum cell-associated fluorescence intensity after 24 h. On the other hand, when treated with folate-decorated Taxol-encapsulating PNPs 11 (▼), a faster increase in cell-associated fluorescence emission was observed, reaching a plateau within 12 h of incubation. Then, the fluorescence intensity rapidly decreases after 12 h of incubation due to the selective induction of apoptosis and therefore reduction in the number of viable fluorescent cells. In contrast, when A549 cells treated with non-folate PNPs (6, ■; 7, ▲) exhibited a nominal increase in cell-associated fluorescence as expected (Figure 5A). In another set of experiments, minimal fluorescence emission was observed when H9c2 cells (FR –) were treated with our functional PNPs (6, ■; 7, ▲; 10, ●; 11, ▼; Figure 5B). These control experiments further confirmed the targeted internalizations and selective fluorescence emissions of our theranostic PNPs. Taken together, these findings support the principle that folate-decorated PNPs can target and deliver chemotherapeutic agents to folate-receptor-expressing carcinomas, in order to prevent damage of nontransformed cells and healthy tissues.

**In Vitro Cellular Uptake of Functional PNPs.** Next, we further investigated the folate receptor-mediated selective uptake and cytotoxicity of our functional PNPs (100 μL, 5.8 nM in PBS, pH = 7.4) by A549 cells (10 000 cells/well) using confocal microscopy. As expected, nominal internalizations were observed when A549 cells were incubated with carboxylated PNPs (6, 24 h of incubation, Figure 6A,B) due to its negatively charged carboxylated surface (zeta potential ζ = –49 mV, Figure S7); however, significant internalization of the folate-conjugated PNPs (10, Figure 6C,D) was indicated as an enhanced fluorescence emission observed from the cell cytoplasm. Interestingly, when A549 cells were incubated with folate-conjugated Taxol-encapsulating PNPs (11), mitotic arrest was observed, leading to a dramatic cellular morphology changes and cell death (Figure 6E,F). Importantly, these confocal microscopic results directly corroborated with our *in vitro* cytotoxicity (Figure 4) and fluorescence spectroscopic (Figure 5) results. In another set of experiments, no internalization of folate-conjugated PNPs 10 was observed (Figure 6G,H), when A549 cells were preincubated with excess of free folic acid, confirming folate receptor-mediated internalizations of our folate-conjugated nanoparticles. In addition, no significant cell-associated fluorescence was observed when H9c2 cells (FR –) were incubated with folate-conjugated PNPs 10 (Figure S10), further confirming folate receptor-mediated internalizations of our functional nanoparticles.

Flow cytometric experiments (FACS, Figure 7) were performed using lung carcinomas (A549 cells: 10 000 cells/well), showing direct corroboration with our previous findings. Results showed nominal cell-associated fluorescence emissions from the A549 cells when incubated with carboxylated PNPs (6, 100 μL, 5.8 nM, in PBS pH = 7.4, 24 h of incubation, Figure 7A), as compared to the control A549 cells (inset, Figure 7A). However, an enhanced cell-associated fluorescence emission was observed for folate-conjugated PNPs (10, Figure 7B), demonstrating folate receptor-targeted cell binding of our theranostic PNPs. In contrast, reduced cell-associated fluorescence was observed when A549 cells were incubated with folate-conjugated Taxol-encapsulating PNPs (11, Figure 7C)

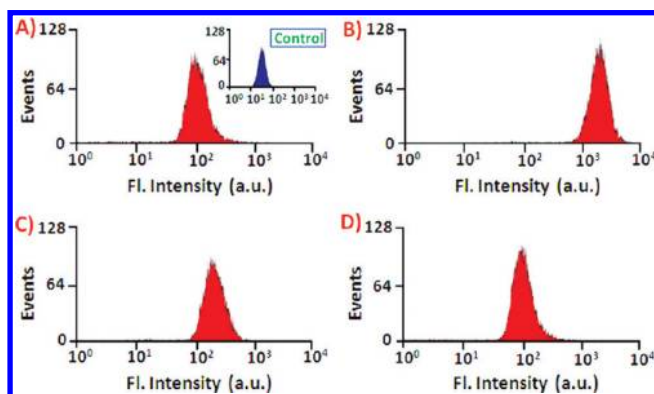


**Figure 7.** *In vitro* flow cytometry analysis of A549 cells incubated with functional PNPs (100  $\mu$ L, 5.8 nM, in PBS pH = 7.4) for 24 h. (A) Nominal fluorescence emission was observed when incubated with carboxylated PNPs (6) compared to the control A549 cells with no treatment (inset). (B) Enhanced fluorescence emission observed for folate-conjugated PNPs (10) whereas, (C) reduced fluorescence emission observed for folate-conjugated Taxol-encapsulating PNPs (11) due to induction of apoptosis. (D) Nominal fluorescence emission was observed for folate-conjugating PNPs (10) in the presence of excess of free folic acid.

for 24 h, indicating target-specific cell binding and delivery of therapeutic drug inducing apoptosis. These results further corroborated with our previous findings: the cytotoxicity (Figure 4), fluorescence spectroscopic (Figure 5), and confocal microscopic (Figure 6) results. In another set of experiments, nominal cell-associated fluorescence emission was observed when A549 cells were preincubated with excess of free folic acid before incubating with folate-conjugating PNPs (10, Figure 7D), indicating exclusive folate receptor-mediated cell binding of our theranostic PNPs. Overall, these results further support the hypothesis that our newly developed theranostic PNPs can target folate receptor-expressing tumors in order to prevent healthy tissues and only induce apoptosis upon receptor-mediated drug delivery.

## CONCLUSIONS

In conclusion, we have introduced a single-step synthetic strategy for the selective *N*-alkylation of amino acids, capable of generating biologically active small molecules. This simple strategy, as opposed to the conventional multistep protection–deprotection method, is facile, highly economic, reproducible, and amenable to scale-up. The resulting functional molecule was used as an AB-type of monomer for the synthesis of biopolymer. The synthesized novel pseudo-poly(amino acid) is different from available linear polymers as its butyl pendants create hydrophobic nanocavities for effective encapsulation of hydrophobic cargos and enhance polymer's solubility in common organic solvent. Utilizing these properties, cargos-encapsulating functional PNPs were synthesized from the resulting amino acid-based polymer, showing promising results in targeted optical detection and treatment of cancer. Particularly, the synthesized Taxol-encapsulating and folate-decorated (using “click” chemistry) theranostic PNPs provided targeted detection and delivery of the therapeutic drug to the folate receptor-expressing cancer cells, resulting in apoptosis, while avoiding healthy, nontransformed tissues. The intracellular fluorescence experiments, cytotoxicity assays, and drug release studies further confirmed for the targeted detection and treatment of cancer. The targeted delivery of the therapeutic

drug to the folate-expressing tumors and induction of apoptosis was monitored using confocal microscopy and flow cytometric analysis. We anticipate that our synthetic strategy may lead to many exciting opportunities for the synthesis of biologically active small molecules, amino acid-based biodegradable polymers, and theranostic polymeric nanoparticles for the targeted delivery of therapeutic agents in clinical settings.

## ASSOCIATED CONTENT

### Supporting Information

Characterizations of the synthesized amino acid-based small molecules, polymer, and theranostic nanoparticles; experimental results using living cells. This material is available free of charge via the Internet at <http://pubs.acs.org>.

## AUTHOR INFORMATION

### Corresponding Author

\*Tel 313-530-4366, e-mail [santra@ucf.edu](mailto:santra@ucf.edu) (S.S.); Tel 407-882-2843, Fax 407-882-2819, e-mail [jmperez@ucf.edu](mailto:jmperez@ucf.edu) (J.M.P.).

## ACKNOWLEDGMENTS

We thank Prof. Anil Kumar, Chemistry Department, IIT Bombay, India, for his advice and help with the organic syntheses and instrumentation facilities. This work was supported by NIH Grant GM 084331 and UCF Start Up Fund, all to J.M.P.

## REFERENCES

- (1) Kim, C. K.; Ghosh, P.; Pagliuca, C.; Zhu, Z. J.; Menichetti, S.; Rotello, V. M. *J. Am. Chem. Soc.* **2009**, *131*, 1360–1361.
- (2) Marder, S. R.; Kippelen, B.; Jen, A. K. Y.; Peyghambarian, N. *Nature* **1997**, *388*, 845–851.
- (3) Nayak, S.; Lee, H.; Chmielewski, J.; Lyon, L. A. *J. Am. Chem. Soc.* **2004**, *126*, 10258–10259.
- (4) Yokoyama, M.; Kwon, G. S.; Okano, T.; Sakurai, Y.; Seto, T.; Kataoka, K. *Bioconjugate Chem.* **1992**, *3*, 295–301.
- (5) You, C. C.; Miranda, O. R.; Gider, B.; Ghosh, P. S.; Kim, I. B.; Erdogan, B.; Krovi, S. A.; Bunz, U. H.; Rotello, V. M. *Nature Nanotechnol.* **2007**, *2*, 318–323.
- (6) Cheng, Z.; Tsourkas, A. *Langmuir* **2008**, *24*, 8169–8173.
- (7) Yadav, S.; van Vlerken, L. E.; Little, S. R.; Amiji, M. M. *Cancer Chemother. Pharmacol.* **2009**, *63*, 711–722.
- (8) Jabr-Milane, L.; van Vlerken, L.; Yadav, S.; Amiji, M. M. *Cancer Treat. Rev.* **2008**, *34*, 592–602.
- (9) Peer, D.; Karp, J. M.; Hong, S.; Farokhzad, O. C.; Margalit, R.; Langer, R. *Nature Nanotechnol.* **2007**, *2*, 751–760.
- (10) Nayak, S.; Lyon, L. A. *Angew. Chem., Int. Ed.* **2005**, *44*, 7686–7708.
- (11) Duncan, R. *Nat. Rev. Drug Discovery* **2003**, *2*, 347–360.
- (12) Frechet, J. M. J.; Henmi, M.; Gitsov, I.; Aoshima, S.; Leduc, M. R.; Grubbs, R. B. *Science* **1995**, *269*, 1080–1083.
- (13) Lee, C. C.; MacKay, J. A.; Frechet, J. M.; Szoka, F. C. *Nature Biotechnol.* **2005**, *23*, 1517–1526.
- (14) Santra, S.; Kaittanis, C.; Perez, J. M. *Langmuir* **2010**, *26*, 5364–5373.
- (15) Kaihara, S.; Matsumura, S.; Mikos, A. G.; Fisher, J. P. *Nature Protoc.* **2007**, *2*, 2767–2771.
- (16) Wang, C.; Ge, Q.; Ting, D.; Nguyen, D.; Shen, H. R.; Chen, J.; Eisen, H. N.; Heller, J.; Langer, R.; Putnam, D. *Nature Mater.* **2004**, *3*, 190–196.
- (17) Jin, C.; Bai, L.; Wu, H.; Song, W.; Guo, G.; Dou, K. *Pharm. Res.* **2009**, *26*, 1776–1784.
- (18) Yuan, M. L.; Wang, Y. H.; Li, X. H.; Xiong, C. D.; Deng, X. M. *Macromolecules* **2000**, *33*, 1613–1617.
- (19) Langer, R. *Nature* **1998**, *392*, 5–10.

- (20) Yokoyama, M.; Miyauchi, M.; Yamada, N.; Okano, T.; Sakurai, Y.; Kataoka, K.; Inoue, S. *Cancer Res.* **1990**, *50*, 1693–1700.
- (21) Mathews, B. T.; Beezer, A. E.; Snowden, M. J.; Hardy, M. J.; Mitchell, J. C. *New J. Chem.* **2001**, *25*, 807–818.
- (22) Nita, L. E.; Chiriac, A. P.; Popescu, C. M.; Neamtu, I.; Alecu, L. *J. Optoelectron. Adv. Mater.* **2006**, *8*, 663–666.
- (23) Crespo, L.; Sancimans, G.; Royo, M.; Giralt, E.; Albericio, F. *Eur. J. Org. Chem.* **2002**, 1756–1762.
- (24) Modica, E.; Zenaletti, R.; Freccero, M.; Mella, M. *J. Org. Chem.* **2001**, *66*, 41–52.
- (25) Garcia-Santos, M. P.; Calle, E.; Casado, J. *J. Am. Chem. Soc.* **2001**, *123*, 7506–7510.
- (26) Adlington, R. M.; Mantell, S. J. *Tetrahedron* **1992**, *48*, 6529–6536.
- (27) Fukuyama, T.; Jow, C. K.; Cheung, M. *Tetrahedron Lett.* **1995**, *36*, 6373–6374.
- (28) Trost, B. M.; Calkins, T. L.; Oertelt, C.; Zambrano, J. *Tetrahedron Lett.* **1998**, *39*, 1713–1716.
- (29) Ebata, M.; Takahashi, Y.; Otsuka, H. *Bull. Chem. Soc. Jpn.* **1966**, *39*, 2535–2538.
- (30) Bar-Haim, G.; Kol, M. *Org. Lett.* **2004**, *6*, 3549–3551.
- (31) Bhatt, U.; Mohamed, N.; Just, G.; Roberts, E. *Tetrahedron Lett.* **1997**, *38*, 3679–3682.
- (32) Bowman, W. R.; Coghlan, D. R. *Tetrahedron* **1997**, *53*, 15787–15798.
- (33) Domling, A.; Ugi, I. I. *Angew. Chem., Int. Ed.* **2000**, *39*, 3168–3210.
- (34) Ohfuné, Y.; Kurokawa, N.; Higuchi, N.; Saito, M.; Hashimoto, M.; Tanaka, T. *Chem. Lett.* **1984**, 441–444.
- (35) Ramanjulu, J. M.; Joullie, M. M. *Synth. Commun.* **1996**, *26*, 1379–1384.
- (36) Reinhold, V. N.; Ishikawa, Y.; Melville, D. B. *J. Med. Chem.* **1968**, *11*, 258–260.
- (37) Song, Y. T.; Sercel, A. D.; Johnson, D. R.; Colbry, N. L.; Sun, K. L.; Roth, B. D. *Tetrahedron Lett.* **2000**, *41*, 8225–8230.
- (38) Tietze, L. F. *Chem. Rev.* **1996**, *96*, 115–136.
- (39) Albanese, D.; Landini, D.; Lupi, V.; Penso, M. *Eur. J. Org. Chem.* **2000**, 1443–1449.
- (40) Kwon, H. Y.; Langer, R. *Macromolecules* **1989**, *22*, 3250–3255.
- (41) Yu, J. H.; Quan, J. S.; Huang, J.; Wang, C. Y.; Sun, B.; Nah, J. W.; Cho, M. H.; Cho, C. S. *Acta Biomater.* **2009**, *5*, 2485–2494.
- (42) McCarthy, J. R.; Perez, J. M.; Bruckner, C.; Weissleder, R. *Nano Lett.* **2005**, *5*, 2552–2556.
- (43) Davis, M. E.; Chen, Z. G.; Shin, D. M. *Nat. Rev. Drug Discovery* **2008**, *7*, 771–782.
- (44) Fonseca, C.; Simoes, S.; Gaspar, R. *J. Controlled Release* **2002**, *83*, 273–286.
- (45) Gupte, A.; Ciftci, K. *Int. J. Pharm.* **2004**, *276*, 93–106.
- (46) Santra, S.; Kaittanis, C.; Grimm, J.; Perez, J. M. *Small* **2009**, *5*, 1862–1868.
- (47) Santra, S.; Kaittanis, C.; Perez, J. M. *Mol. Pharmaceutics* **2010**, *7*, 1209–1222.
- (48) Du, X.; He, J. H. *Mater. Res. Bull.* **2009**, *44*, 1238–1243.
- (49) Texter, J.; Ge, L.; Mourey, T. H.; Bryan, T. G. *Langmuir* **2004**, *20*, 11288–11292.
- (50) Bachovchin, D. A.; Brown, S. J.; Rosen, H.; Cravatt, B. F. *Nature Biotechnol.* **2009**, *27*, 387–394.
- (51) Englert, B. C.; Bakbak, S.; Bunz, U. H. F. *Macromolecules* **2005**, *38*, 5868–5877.
- (52) Kolb, H. C.; Finn, M. G.; Sharpless, K. B. *Angew. Chem., Int. Ed.* **2001**, *40*, 2004–2021.
- (53) Sun, E. Y.; Josephson, L.; Weissleder, R. *Mol. Imaging* **2006**, *5*, 122–128.
- (54) Thorek, D. L. J.; Elias, D. R.; Tsourkas, A. *Mol. Imaging* **2009**, *8*, 221–229.
- (55) Imaz, I.; Hernando, J.; Ruiz-Molina, D.; MasPOCH, D. *Angew. Chem., Int. Ed.* **2009**, *48*, 2325–2329.
- (56) Shi, M.; Wosnick, J. H.; Ho, K.; Keating, A.; Shoichet, M. S. *Angew. Chem., Int. Ed.* **2007**, *46*, 6126–6131.
- (57) Koch, A. M.; Reynolds, F.; Kircher, M. F.; Merkle, H. P.; Weissleder, R.; Josephson, L. *Bioconjugate Chem.* **2003**, *14*, 1115–1121.
- (58) Shen, T.; Weissleder, R.; Papisov, M.; Bogdanov, A. Jr.; Brady, T. J. *Magn. Reson. Med.* **1993**, *29*, 599–604.
- (59) Chan, J. M.; Zhang, L.; Yuet, K. P.; Liao, G.; Rhee, J.-W.; Langer, R.; Farokhzad, O. C. *Biomaterials* **2009**, *30*, 1627–1634.
- (60) Sun, B.; Ranganathan, B.; Feng, S.-S. *Biomaterials* **2008**, *29*, 475–486.
- (61) Danhier, F.; Vroman, B.; Lecouturier, N.; Crockart, N.; Pourcelle, V.; Freichels, H.; Jerome, C.; Marchand-Brynaert, J.; Feron, O.; Preat, V. *J. Controlled Release* **2009**, *140*, 166–173.
- (62) Yu, D.-H.; Lu, Q.; Xie, J.; Fang, C.; Chen, H.-Z. *Biomaterials* **2010**, *31*, 2278–2292.
- (63) Guo, J.; Gao, X.; Su, L.; Xia, H.; Gu, G.; Pang, Z.; Jiang, X.; Yao, L.; Chen, J.; Chen, H. *Biomaterials* **2011**, *32*, 8010–8020.
- (64) Jung, J. H.; Ree, M.; Kim, H. *Catal. Today* **2006**, *115*, 283–287.
- (65) Yoon, S.-A.; Choi, J. R.; Kim, J.-O.; Shin, J.-Y.; Zhang, X.-H.; Kang, J.-H. *Cancer Res. Treat.* **2010**, *42*, 163–171.
- (66) You, J.; Li, X.; Cui, F.; Du, Y.-Z.; Yuan, H.; Hu, F. *Nanotechnology* **2008**, *19*, 1–9.
- (67) Yuan, H.; Miao, J.; Du, Y. Z.; You, J.; Hu, F. Q.; Zeng, S. *Int. J. Pharm.* **2008**, *348*, 137–145.
- (68) Parker, N.; Turk, M. J.; Westrick, E.; Lewis, J. D.; Low, P. S.; Leamon, C. P. *Anal. Biochem.* **2005**, *338*, 284–293.